Supporting information

Highly multiplexed label-free imaging sensor for accurate quantification of small molecule binding kinetics

Elisa Chiodi,[*,†] Allison M. Marn,[†] Matthew T. Geib,[†] Fulya Ekiz Kanik,[†] John Rejman,[‡] David AnKrapp,[‡] and M. Selim Ünlü[†,¶]

†*Department of Electrical Engineering, Boston University, Boston (MA)*

‡*Neogen Corp., Lansing (MI)*

¶*Department of Biomedical Engineering, Boston University, Boston (MA)*

E-mail: elich@bu.edu

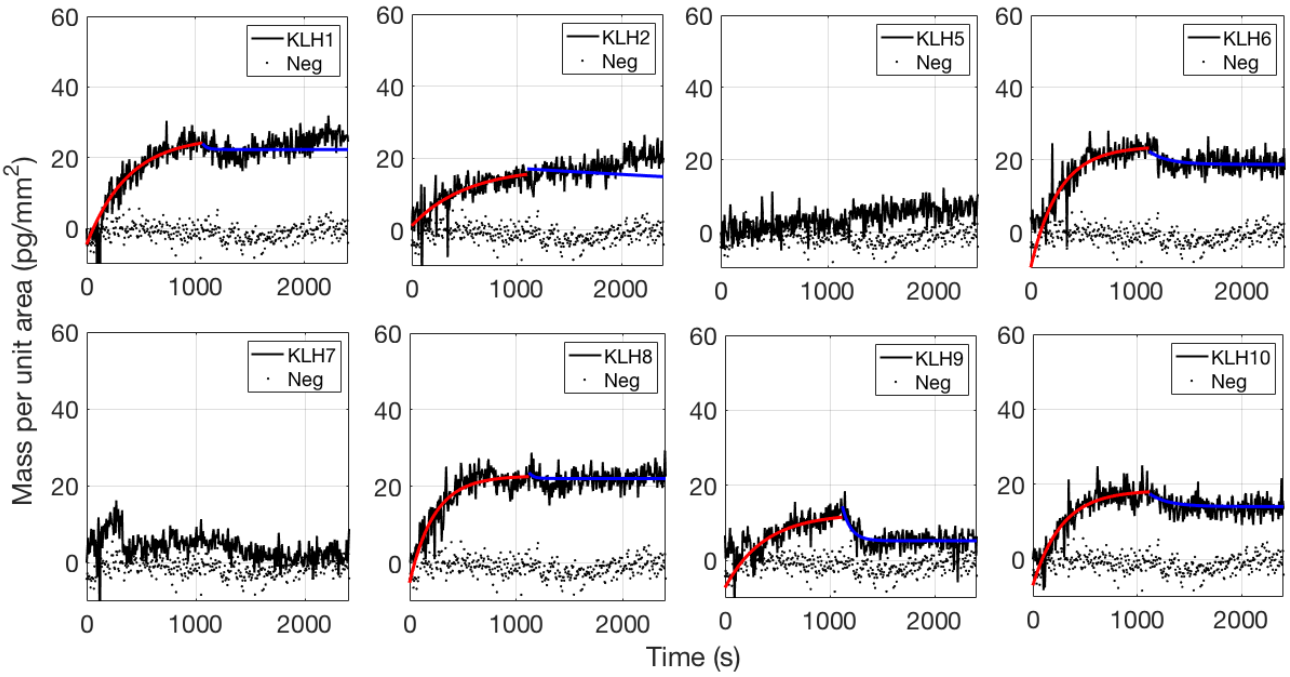

Figure S1: Binding and debinding curves of the fumonisin toxin at a concentration of $100\mu M$ to eight different antibodies generated by immunizing mice with Fumonisin B1 conjugated to Keyhole limpet hemocyanin (KLH); The solid red line indicates the 1:1 fitted association curve, while the solid blue line indicates the fitted dissociation curve. The dotted line represents the control spots' trend.

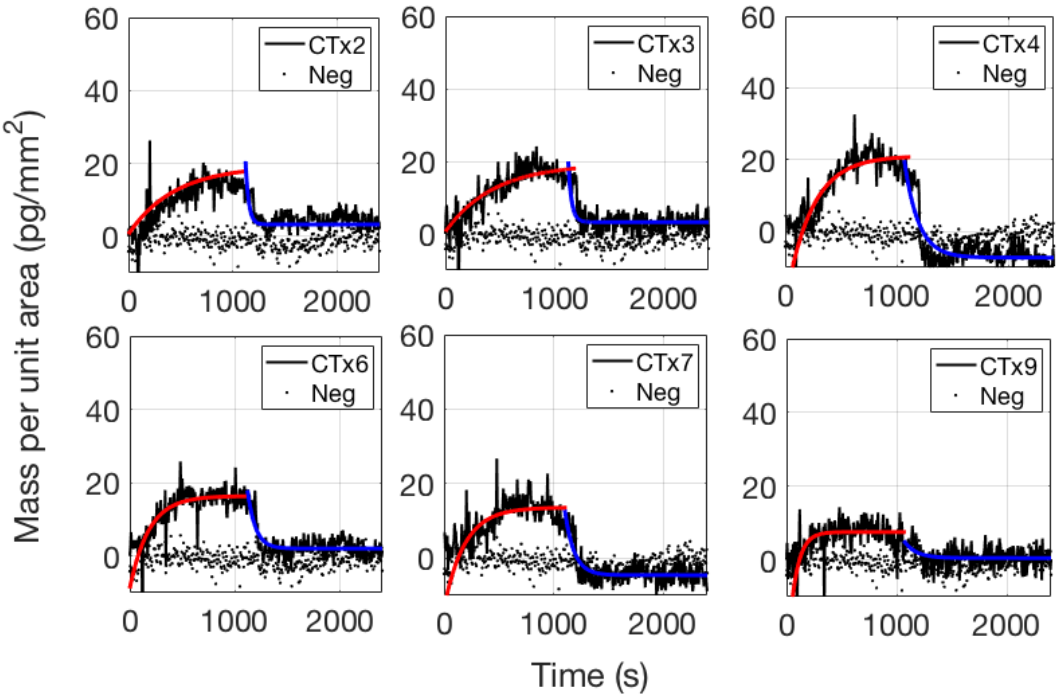

Figure S2: Binding and debinding curves of the fumonisin toxin at a concentration of $100\mu M$ to seven different antibodies generated by immunizing mice with Fumonisin B1 conjugated to Cholera toxin B subunit (CTx-B); The solid red line indicates the 1:1 fitted association curve, while the solid blue line indicates the fitted dissociation curve. The dotted line represents the control spots' trend.

Table S1: Association, dissociation and equilibrium constants calculated for eighteen antibodies against Fumonisin B1, as calculated with a simple 1:1 Langmuir model from the fitted curves of figures 4,S1,S2.

Antibody	$k_{on}(M^{-1}s^{-1})$	$k_{off}(10^{-4}s^{-1})$	$K_D(\mu M)$
CTx-1	15.6 ± 2.2	6.8 ± 3.2	44 ± 22
CTx-2	11.0 ± 2.2	8.8 ± 4.4	80 ± 43
CTx-3	13.1 ± 3.0	9.5 ± 4.3	73 ± 37
CTx-4	27.4 ± 4.6	15.9 ± 4.6	58 ± 19
CTx-5	30.8 ± 2.7	5.1 ± 1.9	17 ± 6
CTx-6	1.1 ± 0.2	53.7 ± 11.8	4986 ± 1461
CTx-7	12.5 ± 4.8	41.1 ± 18.7	329 ± 196
CTx-8	20.0 ± 2.1	5.3 ± 2.1	27 ± 11
CTx-9	31.0 ± 33.4	106 ± 118	341 ± 530
CTx-10	13.6 ± 2.7	3.9 ± 3.2	28 ± 24
KLH-1	8.2 ± 1.5	17.9 ± 4.7	219 ± 70
KLH-2	4.0 ± 0.7	15.2 ± 3.3	377 ± 103
KLH-3	9.3 ± 1.1	14.1 ± 3.0	151 ± 37
KLH-4	31.9 ± 5.7	21.5 ± 5.3	67 ± 22
KLH-5	N/A	N/A	N/A
KLH-6	6.6 ± 0.9	3.0 ± 27.6	46 ± 415
KLH-7	N/A	N/A	N/A
KLH-8	11.9 ± 2.2	31.6 ± 7.5	266 ± 81
KLH-9	10.0 ± 2.8	16.6 ± 7.2	166 ± 85
KLH-10	20.0 ± 3.5	16.1 ± 4.8	81 ± 28

Table S2: Lateral flow assay results for five antibodies screened against Fumoninsin B1

Antibody	TL output (0ppm)	TL output (4ppm)	$B/B_0(\%)$
CTx-3	332562	19366	6%
CTx-7	323101	17089	5%
KLH-2	420017	172564	41%
KLH-7	405429	149375	37%
KLH-9	553577	170125	31%

1 Comparison with theoretically calculated mass density values

For comparison with experimental results we calculated the expected biomass accumulation for a certain range of analyte sizes (in daltons). We simulated a 50-μm radius spot, and we calculated the number of probes immobilized on the surface based on their size and average center-to-center distance. By modeling the molecules as spheres with a diameter in the nm range, we can estimate the biomass accumulation expected for ligands of different molecular weight, both when the immobilized probes form a monolayer on the surface and also for a situation where they are more sparse, which may occur when the spotting concentration is very low. The result of these calculations is presented in Figure S3, with two labels indicating the expected biomass accumulation for Fumonisin B1 ($\approx 27 pg/mm^2$) and for biotin ($\approx 23 pg/mm^2$) on a monolayer of immobilized probes.

The results in Figure S3 stress the fact that having a high density of probes on the surface is fundamental, and therefore spotting optimization procedures need to be considered when the concentration of the spotting solution is very low. This might also be a potential explanation for the lack of detected binding on the KLH5 antibody, whose spotting concentration was so low ($0.46 \mu M$ versus a standard spotting concentration of $7 \mu M$) due to the low purification yield, that the spots were almost invisible. The probes might have been so sparse that even if fumonisin had saturated them, the density on the surface was below the limit of detection (LOD).

To compare these calculated values with experiments, we can consider for example the mean binding density of fumonisin across all the eighteen antibodies, which is $20.9 \pm 7 pg/mm^2$. The huge standard error reflects the fact that fumonisin bound with a different affinity to each antibody, and probably also the difference that the probe concentration on the surface can make. The maximum binding level reached by fumonisin toxin on the CTx8 antibody is indeed $39.8 \pm 2 pg/mm^2$. This value is above the expectations for a monolayer of IgG

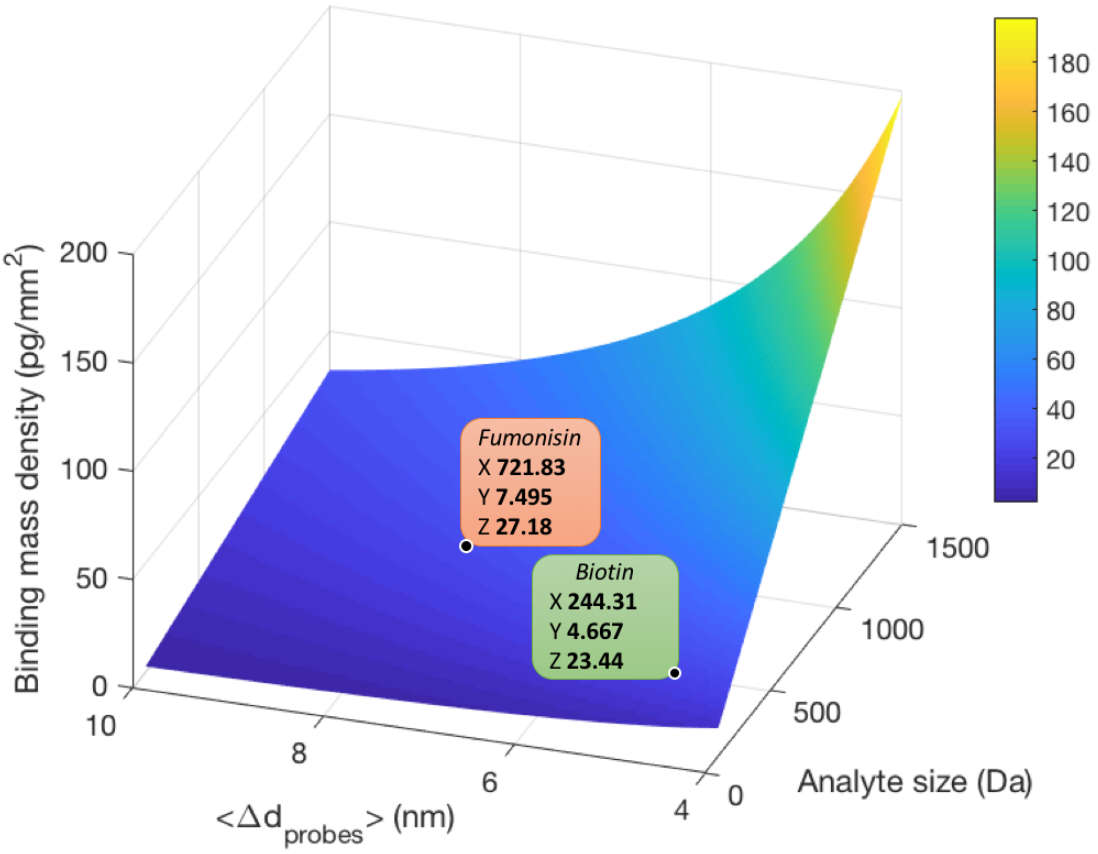

Figure S3: Calculated values for binding mass density for a range of analyte sizes (100-1500Da) and center-to-center average distance between probes (4-10nm). The labels indicate the theoretical values for Fumonisin B1 (red label) and biotin (green label) assuming a monolayer of adjacent probes on a 100μm-sized spot. Streptavidin can be modeled as a 4.66nm-diameter sphere,[1] while IgG antibodies can be assumed to roughly occupy the volume of a 7.5nm-diameter sphere (10nm x 10nm x 2.5nm^2). Therefore, for a monolayer of adjacent probes, their size shall correspond to the average distance between them. The initial mass density increases linearly with the capture probe size. However, we can observe an exponential decrease with increasing distance between probes. This is due to the fact that bigger probes will take up more space on the spot and therefore their number will decrease. Moreover, if the probes are sparse, the binding density will be even less, becoming potentially undetectable.

antibody, which suggests that the tridimensional structure of the polymer matrix might have allowed the probes to overlap, allowing the spot to accommodate slightly more than a monolayer of probes. On the other hand, the experimental result for biotin is $40.3 \pm 1.5 pg/mm^2$, which is almost double the expected value ($\approx 23 pg/mm^2$, Figure S3). The reason for that might be that the simulations have been performed considering a 1:1 interaction between the

capture probe and the analyte. This can be considered realistic for the case of fumonisin: the capture antibody possesses indeed two binding sites for the toxin, but since the orientation of the probe on the surface is random, one of the two sites has a good probability of being inaccessible because it is involved in the immobilization of the molecule (Figure S4b). However, in the case of biotin, every streptavidin molecule has four binding sites, uniformly distributed around the molecule. Therefore, there is a high probability that - on average - two binding sites are available, doubling the biomass accumulation from $\approx 23 pg/mm^2$ to $\approx 46 pg/mm^2$, much closer to the experimental value (Figure S4a).

Moreover, since streptavidin is much smaller than an antibody molecule, a higher number of streptavidin molecules will fit onto a $50 \mu m$-sized spot, and a higher number of biotin molecules will be captured. Therefore, the fact that two biotin molecules are still smaller than one molecule of fumonisin does not necessarily imply that detecting biotin requires more sensitivity than the toxin, because the accumulated mass will be similar or even higher, in accordance with experimental data.

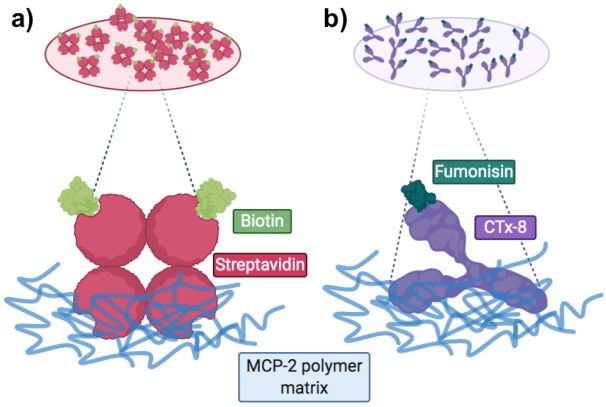

Figure S4: Schematic representation of immobilized streptavidin (a) and fumonisin antibody (b) molecules. Considering the disposition of the binding sites of the molecules, on average, two molecules of biotin will bind to each molecule of streptavidin, while only one molecule of fumonisin will bind to each antibody.

Table S3: The shot noise-related parameters and sensitivity for both the camera used (GS3-U3-51S5M) and the new proposed camera technology (BFS-U3-17S7M). The exposure time is adjusted to fill 75% of the FWC. The temporal resolution $\delta\mathbf{t}$ is currently limited by the computer performance, and is indicated in seconds. Between parentheses is the number of maximum averageable frames. Here, **FF** indicates the Sensor Fill Factor; the **Exp.** header indicates the experimental values, while **Opt.** are the optimal theoretically obtainable values.

Camera	**FWC**	**FPS**	**Sensor Size**	**Sensor FF**		$\delta\mathbf{t}$ (s (fr.))	$\mathbf{\Delta R/R}$		**Biomass** (pg/mm^2)	
GS3-U3-51S5M	10,361	38	5,013,504	**Exp.** 5%	**Opt.** 40%	5 (100)	**Exp.** 4.55e-6	**Opt.** 8.01e-7	**Exp.** 1.8	**Opt.** 0.201
BFS-U3-17S7M	98,645	152	1,760,000	40%		2.6 (400)	2.19e-7		0.55	

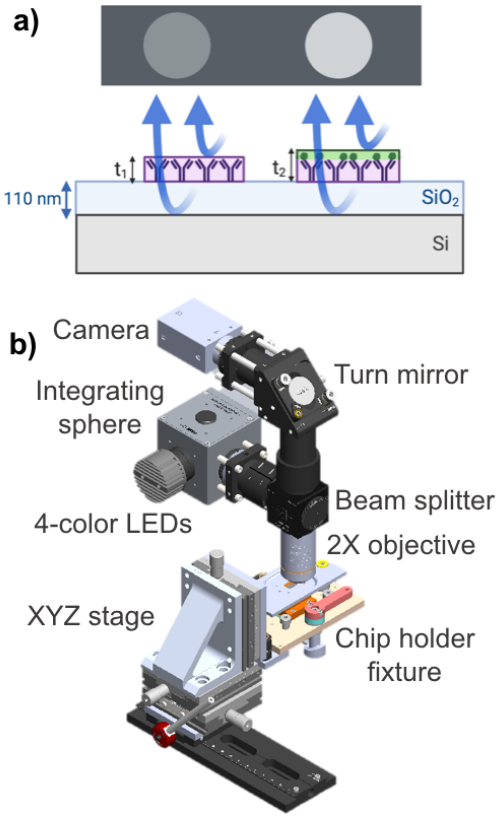

Figure S5: a) The IRIS working principle: biomass accumulation is detected as an increase in signal on the camera sensor, through constructive interference in a common-path interferometer configuration. The substrate (a silicon chip with 110nm of SiO_2 on top) is illuminated from above with a blue (457nm wavelength) LED, and reflectance from the surface through the solution is acquired. A region of the chip that has a thickness $t_2 > t_1$, due to biomass accumulation, will appear brighter on the camera. (b) A rendering of the IRIS setup, where the most important components have been labeled.

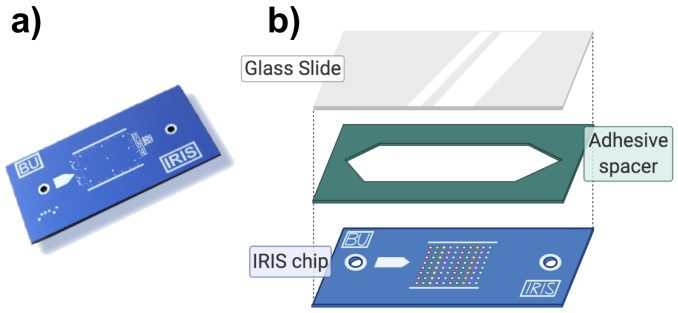

Figure S6: (a) A photo of the Si/SiO_2 IRIS chip and (b) a scheme of the fluidic cartridge used for the experiments. Molecules are immobilized on the surface of the chip in a microarray modality. The chip has drilled through-holes, and is topped with a $130\mu m$ adhesive spacer and a coverglass, forming a channel. In combination with a microfluidics setup, this allows for flowing analyte samples across the surface.

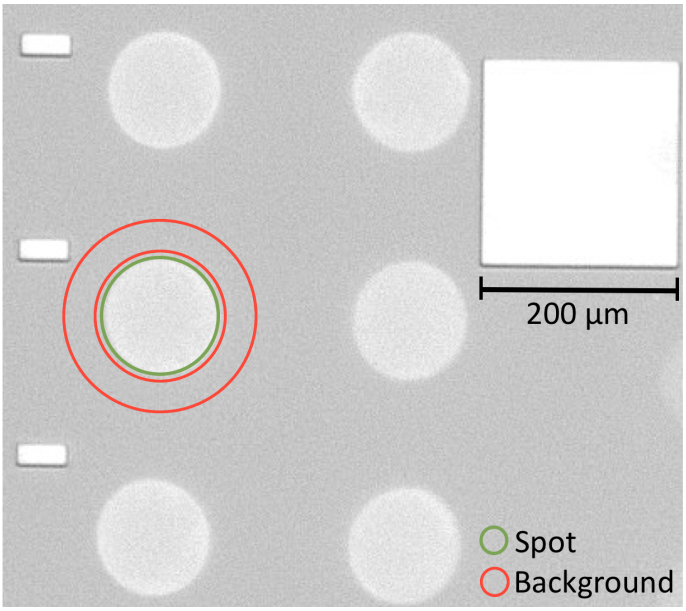

Figure S7: Protein spots on an IRIS chip, where the method of selection of the spot region and background region are highlighted. The signal from the spot (green circle) is averaged and the average signal from the background (red ring) is subtracted to obtain the differential mass accumulation signal. The donut-shaped background allows for precise determination of the thickness difference between the spot and the surrounding region.

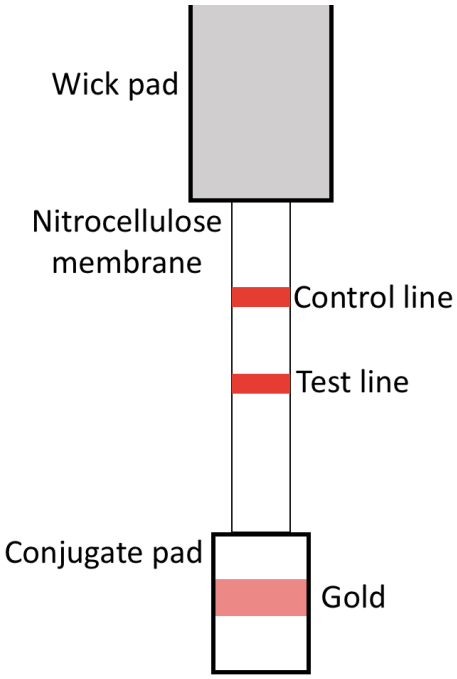

Figure S8: A scheme of the lateral flow assay working principle.

References

(1) Reth, M. Matching cellular dimensions with molecular sizes. *Nat. Immunol.* **2013**, *14*, 765–767.

(2) Williams, E. H.; Davydov, A. V.; Motayed, A.; Sundaresan, S. G.; Bocchini, P.; Richter, L. J.; Stan, G.; Steffens, K.; Zangmeister, R.; Schreifels, J. A.; et al., Immobilization of streptavidin on 4H–SiC for biosensor development. *Appl. Surf. Sci.* **2012**, *258*, 6056–6063.